Effect of Intra-particle Conduction and Surface Subdivision on High-Temperature Thermal Analysis

Sohyeon Ahn [a], Eung Soo Kim [a*]
[a] *Nuclear Engr. Dept., Seoul National Univ., 1 Gwanak-ro, Gwanak-gu, Seoul 08826, Republic of Korea*
[*] *Corresponding author: kes7741@snu.ac.kr*

***Keywords :** Radiative heat transfer, Intra-particle conduction, Monte Carlo Ray Tracing, DEM, Dimensionless solid conductivity

1. Introduction

In Pebble Bed Reactors (PBRs), fuel temperatures can reach up to 1900 K [1] during transients, making radiative heat transfer a dominant thermal mechanism. Traditional approaches, such as the Zehner-Bauer-Schlünder (ZBS) model [2], treated the packed bed as a continuum to estimate effective thermal conductivity. While subsequent Discrete Element Method (DEM) and Voronoi-based models improved the representation of structural heterogeneities, they remained restricted to "short-range" radiative interactions and the "isothermal particle" (thermally lumped) assumption [3-5].

Recent studies indicate that these approximations fail at elevated temperatures, where fourth-power radiation scaling induces significant intra-particle temperature gradients and long-range exchange [6-8]. Although "microscopic models" have been proposed to resolve these gradients by subdividing particle surfaces, their widespread application is hindered by extreme computational costs.

To address these coupled challenges, this study presents a high-fidelity thermal model that integrates long-range radiative exchange via Monte Carlo Ray Tracing (MCRT) with detailed intra-particle conduction. By leveraging GPU-based parallelization within a DEM framework, the proposed model captures dynamic particle motion and non-isothermal surface effects at a tractable computational cost, providing a more accurate subdivision criterion for high-temperature PBR analysis.

A parametric study on particle subdivision and the effective thermal conductivity of the packed bed demonstrates the discretization requirements for accurate high-temperature predictions. Finally, we propose a material-independent subdivision criterion defined by a dimensionless parameter that integrates solid conductivity and emissivity.

2. Methodology

2.1. Monte Carlo Ray Tracing (MCRT)

In Pebble Bed Reactors (PBRs), the fuel elements consist of opaque materials with optically diffuse, rough graphite surfaces, while the void spaces are filled with non-participating, transparent helium gas. This environment makes surface-to-surface view factors effective for modeling radiative heat transfer. However, deterministic view factor computation is highly inefficient due to the severe geometric occlusion and shadowing inherent in closely packed pebble beds. To circumvent this, the Monte Carlo Ray Tracing (MCRT) method is utilized to stochastically evaluate radiative exchange.

The total radiation emitted from surface i and striking surface j is calculated using the Stefan-Boltzmann law combined with the view factor $F_{i\to j}$.

$$Q_{i\to j} = F_{i\to j}\varepsilon_i \sigma A_i T_i^4 \tag{1}$$

The Monte Carlo Ray Tracing (MCRT) method stochastically computes these view factors to handle the geometric complexity and shadowing of the packed bed. The ray tracing algorithm consists of the following key steps.

(1) Ray origin: Random numbers Θ and Φ uniformly distributed in the range 0 to 1 are generated to define the origin point coordinates on the spherical segment.

$$\theta = \cos^{-1}(2\Theta - 1), \phi = 2\pi\Phi \tag{2}$$

$$X = (R\sin\theta\cos\phi, R\sin\theta\sin\phi, R\cos\phi) \tag{3}$$

(2) Ray direction: Kowsary's tangent sphere method [9] is utilized to sample directions, where a second point is randomly generated on a hypothetical sphere tangent to the origin.

(3) Intersection Detection: Ray-surface intersections are determined by evaluating the discriminant of a quadratic equation representing a ray striking a bounding sphere.

$$\text{Intersection: } \left|\boldsymbol{X} + t\boldsymbol{Y} - \boldsymbol{C}_j\right| \le R_j \; with \; t > 0 \tag{4}$$

(4) View Factor Calculation: The fraction of rays emitted from surface i that strike surface j defines the view factor. A symmetry correction is applied subsequently to ensure reciprocity.

$$A_i F_{i\to j} = A_j F_{j\to i} = \left(A_i F_{i\to j} + A_j F_{j\to i}\right)/2 \tag{5}$$

Due to the rough graphite surfaces and relatively small temperature differences between neighbors, Kirchhoff's law applies, meaning absorptivity equals emissivity. The rough graphite surface is assumed to be fully diffusive,

where the reflected radiative flux is directed isotropically over the hemisphere. Consequently, the net radiative heat transfer to surface i is expressed in terms of the irradiation G and the fraction of the emitted radiative energy that is ultimately absorbed S.

$$Q_i = \varepsilon_i A_i G_i - \varepsilon_i A_i \sigma T_i^4 S_i \quad (6)$$

$$G_i = \sum F_{i\to j}(\varepsilon_j \sigma T_j^4 + (1-\varepsilon_j)G_j) \quad (7)$$

$$S_i = \sum F_{i\to j}(\varepsilon_j + (1-\varepsilon_j)S_j) \quad (8)$$

While the contributions from reflection require recursive accumulation of radiative exchange terms, the number of reflections considered must be appropriately limited based on surface emissivity to maintain computational feasibility.

2.2. Discrete Element Method (DEM)

The mechanical behavior and conductive heat transfer resulting from particle overlap are tracked using the Discrete Element Method (DEM). Momentum exchange is calculated via the Hertz-Mindlin contact force model, which divides forces into normal (n) and tangential (t) components, each containing spring (s) and dashpot (d) contributions [10,11].

$$F_{ab} = f_{ab}^n \hat{n} + f_{ab}^t \hat{t} = (f_s^n + f_d^n)\hat{n} + (f_s^t + f_d^t)\hat{t} \quad (9)$$

Inter-particle heat exchange is processed using Batchelor's model, which defines heat flux based on the effective matrix conductivity (k_{ab}) and the radius of the flat contact circle (r_c) [12].

$$Q_{ab} = 2k_{ab} r_c (T_a - T_b) \quad (10)$$

The contact radius is derived from the normal overlap (δ_n) and the effective particle radius (r_p) using the relation $r_c = \sqrt{2\delta_n r_p - \sigma_n^2}$.

2.3. Integrated thermal model

To capture high-temperature thermal gradients accurately, the model implements intra-particle subdivision. As visualized in the manuscript's Figure 1, each particle is geometrically discretized into angular sectors and concentric radial layers, forming a set of control volume segments.

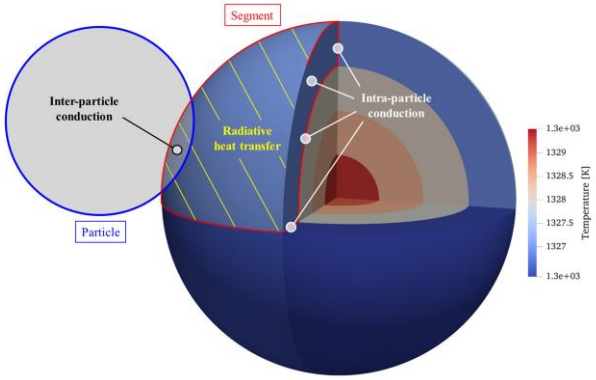

Fig. 1. Schematic of integrated thermal model.

Outermost segments define surface control volumes that engage in both radiative exchange and DEM-based inter-particle contact conduction. Internal segments transfer heat via radial and angular diffusion governed by Fourier's law.

$$Q_{ij} = -\frac{2}{k_i^{-1} + k_j^{-1}} A_{ij} \frac{T_i - T_j}{D_{ij}} \quad (12)$$

The integrated computational framework operates iteratively. According to the flowchart in the manuscript's Figure 2, the process begins with a Nearest Neighbor Particle Search (NNPS) to establish spatial proximity. If geometric changes trigger it, the MCRT module updates the limited neighbor list and view factors. A coupled thermo-mechanical loop then advances the integrated thermal state, updates thermal expansion, and recomputes particle interactions via DEM. All major operations are highly parallelized on GPUs to mitigate the computational burden of resolving thousands of ray traces and particle sub-volumes.

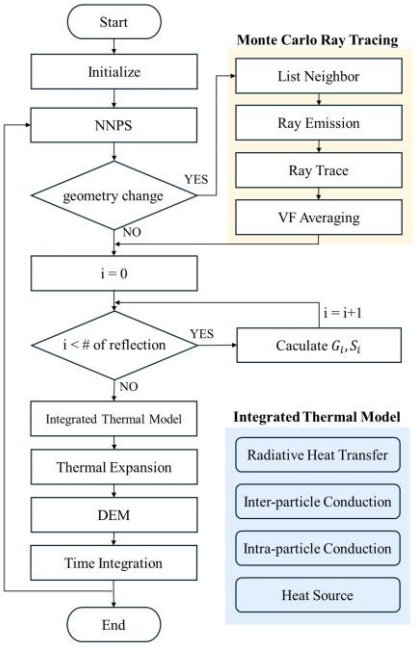

Fig. 2. Flowchart of integrated thermal model.

3. Results and Discussion

3.1. Validation of integrated thermal model

The integrated thermal model was validated by predicting the effective thermal conductivity (ETC) of mono-sized packed beds. In the simulations, a constant downward heat flux is applied at the top boundary while the bottom is fixed at an initial reference temperature. Once steady-state conditions manifest, a linear axial temperature gradient forms, enabling the evaluation of macroscopic thermal properties based on Fourier's law.

The simulation outputs were compared against experimental vacuum conditions for both graphite and ZrO_2 beds. For graphite, the model maintained high predictive accuracy up to approximately 1900 K, a critical regime where traditional short-range approximations usually fail. For the ZrO_2 configurations, the generated model envelope successfully encapsulated the experimental measurements [13-14], reflecting the consistency of the framework against reported variability in solid property data.

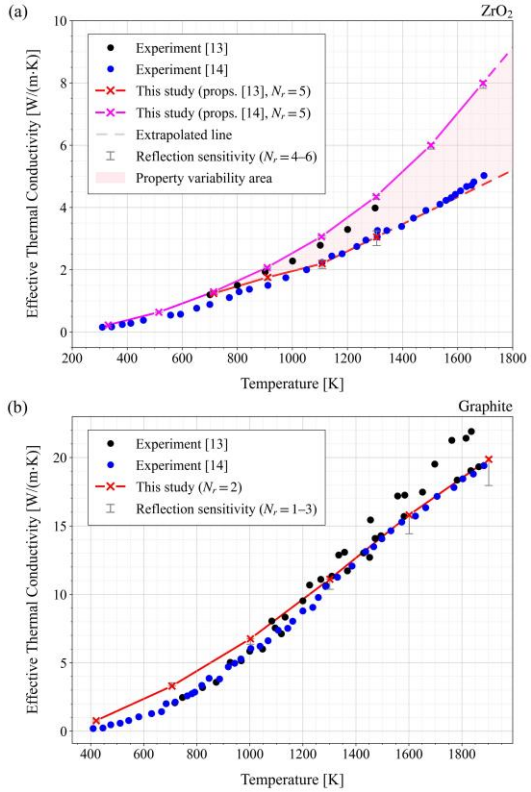

Fig. 3. Validation of Integrated thermal model

3.2. Parametric Study

To determine when intra-particle discretization is mandatory, a parametric study explored the impact of the Dimensionless Solid Conductivity (DSC). Specifically, a modified, material-independent parameter (Λ_ϵ) was formulated to compare internal solid conduction directly to surface radiation.

$$\Lambda_\varepsilon = \frac{k_s}{4\sigma\varepsilon d_p T_s^3} \tag{13}$$

Physically, Λ_ε functions as a radiative Biot-type number, representing the relative magnitude of the effective radiative conductivity ($k_{rad} = 4\varepsilon\sigma d_p T_s^3$) compared to the solid conductivity (k_s). When $\Lambda_\varepsilon \ll 1$, internal conduction dominates, effectively minimizing internal temperature gradients. In this regime, the particle can be treated as isothermal, and further spatial subdivision is unnecessary. Conversely, for $\Lambda_\varepsilon \gg 1$, internal conduction is limited relative to surface radiation, leading to significant temperature non-uniformity. In such cases, fine subdivision of the particle is essential to accurately capture the internal thermal gradients.

Based on this interpretation, we conducted a parametric study to investigate the correlation between Λ_ε and the required level of discretization. Four geometric models were tested against experimental data: Fully resolved, Angular + surface layer, Angular only, and Lumped (isothermal). Plotting the models against Λ_ϵ produced a universal correlation.

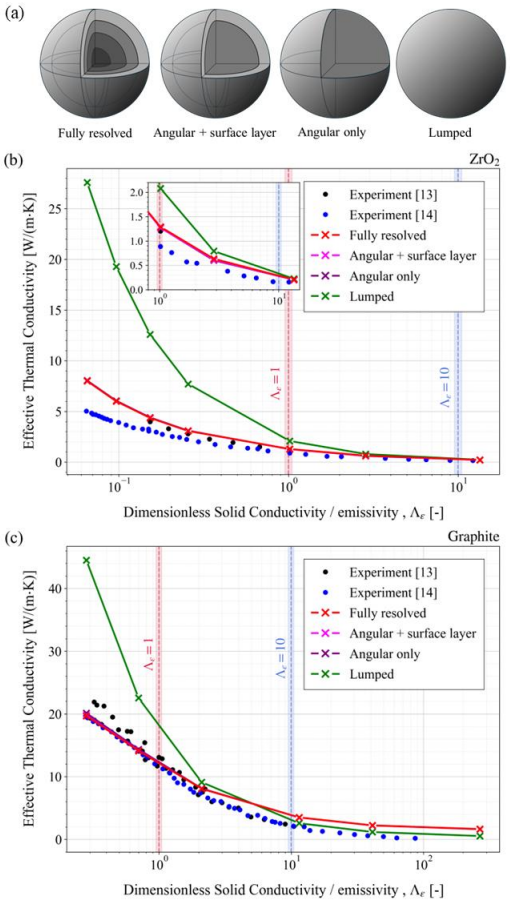

Fig. 4. Parametric *study on particle subdivision*

The result demonstrates that, despite difference in absolute values across materials, the computed effective thermal conductivity follows a consistent trend when plotted against Λ_ϵ. This confirms its role as a material-

agnostic, universal criterion for evaluating the necessity of particle discretization.

In the non-isothermal regime ($\Lambda_\epsilon < 1$), the lumped model significantly overestimates the effective thermal conductivity due to its inability to resolve internal thermal resistance. However, as Λ_ϵ increase beyond unity, the discrepancy between the subdivision models diminishes, and the curves nearly coincide for $\Lambda_\epsilon \gg 1$. In this isothermal limit, the influence of subdivision becomes negligible, validating the use of a lumped isothermal volume to represent each particle.

Further analysis distinguishes the specific contributions of angular and radial subdivision. Angular partitioning addresses the bias introduced by non-uniform radiosity on the pebble surface and is the dominant factor at high temperatures. As observed in the results, the "Angular only" model captures the majority of non-isothermal effects, while the addition of radial layers yields only marginal improvements in stagnant bed configurations. Consequently, while angular segmentation should be prioritized to account for intra-particle conduction, radial discretization remains a secondary requirement, becoming essential primarily for pebbles with internal heat generation or layered coatings that induce steep radial temperature gradients.

4. Conclusion

This study successfully established a high-fidelity thermal model coupling MCRT radiation with DEM contact mechanics, enabling the resolution of surface temperature gradients within pebble beds. A rigorous parametric study yielded a material-independent subdivision criterion (Λ_ϵ) that governs when internal conduction significantly impacts macroscopic heat transfer behavior.

The findings confirm that defining particles as uniform, lumped spheres is sufficient only when $\Lambda_\epsilon > 10$, as internal conduction prevents severe surface gradients. Conversely, intra-particle subdivision becomes essential as the parameter approaches unity, and is strictly mandatory when $\Lambda_\epsilon < 1$. Additionally, the analysis revealed that angular segmentation primarily mitigates prediction biases caused by non-uniform radiosity, while radial layering offers only minor corrections for stagnant, unheated packed beds. By deploying GPU acceleration and defining rigorous discretization thresholds, this integrated framework provides a robust and computationally feasible tool for predicting reliable core temperatures under extreme high-temperature operating conditions.

ACKNOWLEDGMENTS

This research was supported by the National Research Council of Science & Technology(NST) grant by the Korea government (MSIT) (No. GTL24031-000). This work was supported by the Korea Institute of Energy Technology Evaluation and Planning(KETEP) and the Ministry of Trade, Industry & Energy(MOTIE) of the Republic of Korea (No. RS-2024-00487321).

REFERENCES

[1] F. Reitsma, G. Strydom, J. De Haas, K. Ivanov, B. Tyobeka, R. Mphahlele, et al., The PBMR steady-state and coupled kinetics core thermal-hydraulics benchmark test problems, Nucl. Eng. Des, Vol. 236, pp. 657–668, 2006.
[2] R. Bauer, E. Schlünder, Effective radial thermal conductivity of packings in gas flow – 2. Thermal conductivity of the packing fraction without gas flow, Int. Chem. Eng, Vol. 18, pp. 189–204, 1978.
[3] D. Vortmeyer, Wärmestrahlung in Kugelschüttungen, VDI-Fortschrittsberichte, Reihe 3, 1966.
[4] M. de Beer, P.G. Rousseau, C.G. du Toit, A review of methods to predict the effective thermal conductivity of packed pebble beds, with emphasis on the near-wall region, Nucl. Eng. Des, Vol. 331, pp. 248–262, 2018.
[5] W. van Antwerpen, P.G. Rousseau, C.G. du Toit, Multi-sphere unit-cell model to calculate the effective thermal conductivity in packed pebble beds of mono-sized spheres, Nucl. Eng. Des, Vol. 247, pp. 183–201, 2012.
[6] H. Wu, N. Gui, X. Yang, J. Tu, S. Jiang, Effect of scale on the modeling of radiation heat transfer in packed pebble beds, Int. J. Heat Mass Transf, Vol. 101, pp. 562–569, 2016.
[7] T. Pitso, Characterisation of long-range radiation heat transfer in packed pebble beds, Ph.D. Thesis, North-West University, Potchefstroom, South Africa, 2011.
[8] Y. Liu, X. Zhang, H. Wang, Particle non-isothermality effect on the radiative thermal conductivity in dense particulate systems, Int. J. Heat Mass Transf, Vol. 186, 2022.
[9] F. Kowsary, Technical Note a computationally efficient method for Monte Carlo simulation of diffuse radiant emission or reflection, Int. J. Heat Mass Transf, Vol. 42, pp. 193–195, 1999.
[10] R.D. Mindlin, H. Deresiewicz, Elastic spheres in contact under varying oblique forces, J. Appl. Mech, Vol. 20, pp. 327–344, 1953.
[11] Y.B. Jo, S.H. Park, H.S. Yoo, E.S. Kim, GPU-based SPH-DEM method to examine the three-phase hydrodynamic interactions between multiphase flow and solid particles, Int. J. Multiph. Flow, Vol. 153, 2022.
[12] Z.Y. Zhou, A.B. Yu, P. Zulli, A new computational method for studying heat transfer in fluid bed reactors, Powder Technol, Vol. 197, pp. 102–110, 2010.
[13] G. Breitbach, H. Barthels, The radiant heat transfer in the high-temperature reactor core after failure of the afterheat removal systems, Nucl. Technol, Vol. 49, pp. 392–399, 1980.
[14] K. Robold, Heat transfer in the inner and boundary region of pebble beds, Dissertation, Kernforschungsanlage Jülich GmbH, IRB Jül-1796, 1982.